Photoacoustics 21 (2021) 100239

Contents lists available at ScienceDirect

Photoacoustics

journal homepage: www.elsevier.com/locate/pacs

Research article

A novel photoacoustic-fluorescent contrast agent for quantitative imaging of lymphatic drainage

Kirsten Cardinell [a,b,c], Neeru Gupta [a,b,d,g,h], Bryan D. Koivisto [i], J. Carl Kumaradas [c], Xun Zhou [a,b], Hyacinth Irving [a], Paola Luciani [j], Yeni H. Yücel [a,b,c,d,e,f,*]

[a] Keenan Research Centre for Biomedical Science, Li Ka Shing Knowledge Institute, St. Michael's Hospital, Unity Health Toronto, Toronto, Ontario, Canada
[b] Department of Ophthalmology and Vision Sciences, St. Michael's Hospital, Unity Health Toronto, University of Toronto, Toronto, Ontario, Canada
[c] Department of Physics, Faculty of Science, Ryerson University, Toronto, Ontario, Canada
[d] Department of Laboratory Medicine & Pathobiology, St. Michael's Hospital, University of Toronto, Toronto, Ontario, Canada
[e] Institute of Biomedical Engineering, Science and Technology (iBEST), St. Michael's Hospital, Ryerson University, Toronto, Ontario, Canada
[f] Department of Mechanical Engineering, Faculty of Engineering and Architectural Science, Ryerson University, Toronto, Ontario, Canada
[g] Glaucoma Unit, St. Michael's Hospital, Unity Health Toronto, Toronto, Ontario, Canada
[h] Dalla Lana School of Public Health, University of Toronto, Toronto, Ontario, Canada
[i] Department of Chemistry and Biology, Ryerson University, Toronto, Ontario, Canada
[j] Department of Chemistry, Biochemistry, and Pharmaceutical Sciences, University of Bern, Freiestrasse 3, CH-3012, Bern, Switzerland

ARTICLE INFO

Keywords:
Contrast agent
Minimum detectable concentration
Limit of detection
Linear range
Photobleaching
Photostability
Fluorescence imaging
Lymphatic imaging
Near-infrared

ABSTRACT

In vivo near-infrared (NIR) photoacoustic imaging (PAI) studies using novel contrast agents require validation, often *via* fluorescence imaging. Bioconjugation of NIR dyes to proteins is a versatile platform to obtain contrast agents for specific biomedical applications. Nonfluorescent NIR dyes with higher photostability present advantages for quantitative PAI, compared to most fluorescent NIR dyes. However, they don't provide a fluorescence signal required for fluorescence imaging. Here, we designed a hybrid PA-fluorescent contrast agent by conjugating albumin with a NIR nonfluorescent dye (QC-1) and a visible spectrum fluorescent dye, a BODIPY derivative. The new hybrid tracer QC-1/BSA/BODIPY (QBB) had a low minimum detectable concentration (2.5μM), a steep linear range (2.4–54.4 μM; slope 3.39 E -5), and high photostability. Tracer signal was measured *in vivo* using PAI to quantify its drainage from eye to the neck and its localization in the neck lymph node was validated with postmortem fluorescence imaging.

1. Introduction

The lymphatic system drains excess fluid and solutes from the interstitial tissue into lymph nodes, and is involved in cancer spread [1], inflammation [2], diabetes [3], and obesity [4]. Furthermore, the lymphatic system has recently been linked to a fluid drainage pathway in the eye [5,6]. The analysis of the ocular drainage rate into the lymphatic system can potentially be used as a measure for the effectiveness of existing and novel glaucoma treatments [7]. Photoacoustic imaging (PAI) has previously been used for visualization and quantification of lymph node imaging [8–13] and lymphatic drainage from the eye [14,15].

PAI can provide anatomical and functional information with high resolution by probing a wide variety of endogenous absorbers including hemoglobin, and melanin. However, to visualize the lymph, a clear, non-absorbing bodily fluid [16], the use of an exogenous PA contrast agent is required. Near-infrared (NIR) dyes are often used as the signaling component of a PA contrast agent. NIR dyes have low toxicity and can be conjugated to various proteins and antibodies without altering their targeting properties [17]. Albumin, a ubiquitous plasma protein that is approved for multiple medical applications by the Food and Drug Administration, can be readily bioconjugated with NIR dyes to enhance their solubility, bioavailability, and biocompatibility [18]. Albumin is also frequently used as the carrier in fluorescence [14,19] and PA [7,20] lymphatic studies.

Since PA images are generated with computer-based reconstruction and spectral unmixing algorithms applied to the PA signal, *in vivo* PAI in biology and pathology applications often requires validation by

* Corresponding author at: Keenan Research Centre for Biomedical Science, St. Michael's Hospital, Unity Health Toronto, 30 Bond Street, 209 LKSKI Room 409, Toronto, Ontario M5B 1W8, Canada.
E-mail address: yeni.yucel@unityhealth.to (Y.H. Yücel).

https://doi.org/10.1016/j.pacs.2021.100239
Received 4 June 2020; Received in revised form 20 November 2020; Accepted 5 January 2021
Available online 8 January 2021

postmortem *in situ* and histological studies [21–26]. Fluorescence imaging [27] is helpful to validate the location of tracers detected in *in vivo* PAI especially when testing novel dyes and spectral unmixing techniques. Fluorescence imaging may also be used to assess the biodistribution of a contrast agent within various organs, its potential toxicity, and its interaction with the immune system [28–30].

For validation studies, the detection of contrast agents using both PA and fluorescence imaging modalities in the same animal would require contrast agents that contain either a NIR fluorescent dye, or both a NIR nonfluorescent dye and a fluorescent dye.

Recent studies have shown superior characteristics of nonfluorescent dyes over some fluorescent ones for use in PAI [17,31,32]. Nonfluorescent (dark) NIR quencher dyes with a near-zero fluorescence quantum yield and higher photostability may be more advantageous for sequential quantitative PAI.

One NIR dye, a nonfluorescent contrast agent, IRDye QC-1® (QC-1) enables higher detection of malignancies when compared to ICG with PAI [33], and was previously conjugated to albumin for quantitative lymphatic PAI [7,20]. However, imaging approaches to localize fluorescent tracers cannot be effectively applied to dark quencher contrast agents due to their lack of fluorescence. To address this challenge, we developed a hybrid contrast agent that provides near equivalent or better PA contrast to QC-1 with fluorescence properties.

We obtained a contrast agent with the PA, fluorescence, and tracing properties that are required for our experiments by labeling the lymph targeting albumin protein with a NIR dark quencher dye for the PA signal generation as well as a fluorescent dye. The ideal fluorescent dye for our application requires a peak fluorescence emission wavelength below the quenching range (approximately 550–950 nm) of the quencher dye to avoid quenching of the fluorescent signal. Additionally, the fluorescent dye benefits from absorption wavelengths below the PAI range to avoid unnecessary photobleaching of the fluorescence signal. A strong candidate for such a fluorescent dye in the visible (VIS) range is BODIPY which is known for its high molar extinction coefficient and quantum yield [34]. In addition, the fluorescence signal of BODIPY at 488 nm can be detected by the fluorescence microscopes and scanners that are readily available in most biomedical facilities.

In this paper, we aim to design and characterize a hybrid contrast agent for both quantitative PAI and qualitative visible fluorescence imaging of ocular lymphatic clearance. The contrast agent is composed of albumin to target the lymph nodes, a NIR dye to provide PA contrast, and a VIS fluorescent dye to provide a fluorescence signal for postmortem validation. To select the NIR dye for the hybrid contrast agent we systematically compare commercial dyes with NIR absorbance (680–980 nm) with optimal characteristics for sequential quantitative PAI. These characteristics include high extinction coefficients, low minimum detection limit, large and steep linear ranges, and strong PA photostability during prolonged NIR laser exposure from PAI. Albumin, after the conjugation with the selected NIR dye, is conjugated with a VIS fluorescent dye. Similar quantitative assays are performed for the hybrid dual-modality PA-fluorescent contrast agent. This novel hybrid contrast agent is then tested *in vivo* with PAI to observe lymphatic drainage over time in mice and its location in the lymph node is validated with postmortem *in situ* fluorescence imaging and microscopy.

If FDA approved, hybrid contrast agents similar to that described here could translate to the clinic with use alongside readily available clinical devices with a fluorescein imaging channel. Applications include but are not limited to eye imaging [7,20] and lymphatic imaging in cancer in patients [35,36].

2. Materials and methods

2.1. Comparison of NIR dyes for photoacoustic imaging

We compared three commercially available NIR dyes including IRDye QC-1, IRDye 800CW, and CF770, with peak absorption wavelengths well within the NIR range of the PAI system used in this study. We determined their minimum detectable concentrations (MDC), relationships between concentration and PA signals (linear ranges), and changes in PA signal over time with repetitive PAI (PA photostability) in a systematic manner as described in the Supplementary Material. Although the NIR dyes showed comparable MDCs, QC-1 was selected as the NIR PA signaling compound for the hybrid contrast agent due to its steeper slope for the linear range and superior photostability compared to the other 2 dyes (Supplementary Material section 4).

2.2. Hybrid dye preparation

For the hybrid contrast agent preparation, QC-1 dye was conjugated to bovine serum albumin (BSA; Sigma-Aldrich, USA; MW: 66.4 kDa) following the manufacturer's protocol (IRDye 800CW Protein Labeling Kit-High MW, LI-COR Biosciences). QC-1/BSA was then mixed with BODIPY maleimide (ex: 504 nm, em: 510 nm, B10250, ThermoFisher Scientific, Canada) in phosphate buffer and incubated at room temperature for 2 h without light. After each conjugation step, the mixtures were filtered with a 3 kDa Amicon Ultra-15 Centrifugal Filter Unit (Sigma-Aldrich, MO, USA) to remove any free dye. The final mixture was concentrated using a centrifugal concentrator (Vivaspin Turbo 15, Sartorius, Canada). The hybrid QC-1/BSA/BODIPIY (QBB) tracer absorbance was measured using a plate reading spectrophotometer (Multi-Mode Reader Synergy Neo2, BioTek, VT, USA) to determine the final concentration. The peak absorbance at 750 nm associated with the QC-1 component of the QBB tracer was used to determine the concentration. Absorbance spectra of QBB and its components were used to calculate the dye to protein ratios and the calculation is shown in Supplementary Material Section 3.

The QBB tracer was diluted to 16 concentrations in PBS (200, 175, 150, 120, 100, 75, 50, 25, 20, 10, 5, 2.5, 1.25, 0.625, 0.313, and 0.156 μM). Absorbance spectrum measurements were taken with the same plate reading spectrophotometer. Absorbance was measured for duplicate samples from 680 nm to 980 nm in 1 nm steps and the concentrations were calculated using the Beer-Lambert law.

2.3. In vitro photoacoustic imaging

Tracer concentrations were imaged in capillary tubes cut to 3.5 cm (Inner diameter of 1.1 mm and outer diameter of 1.5 mm, Thermo Fisher Scientific, ON, Canada) within a light scattering, non-absorbing cylindrical agar phantom next to a PBS filled capillary tube as described in Yucel et al. [24]. Phantoms with varying concentrations of the tracer were imaged using the MSOT inVision 128 (iThera Medical GmbH, Munich, Germany).

Two experiments were performed. The first experiment was performed to determine the minimum detectable concentration (MDC) and linear range, the phantoms with each concentration were imaged using wavelengths from 680 to 980 nm in 5 nm steps every 2 mm along the z-axis of the capillary tubes. The second experiment was performed to assess PA photostability, we imaged only one concentration (25 μM) at its maximum absorption wavelength every 0.5 mm along the z-axis of the capillary tubes. Both experiments imaged triplicate samples per concentration.

2.4. In vitro data analysis

PA images were reconstructed using the Backprojection algorithm within the native ViewMSOT software (v3.8; iThera Medical GmbH). For the first experiment only, the images were spectrally unmixed with the Linear Regression algorithm in ViewMSOT. For both experiments, regions of interest (ROIs) were taken surrounding both the capillary tubes, and the mean pixel intensity (MPI) within the ROIs were recorded. All *in vitro* analysis was also performed on free NIR dyes and these results are shown in Supplementary Material section 4.

2.4.1. Minimum detectable concentration calculation

The limit of detection (LOD, $L_{detection}$) *in vitro* was calculated using EP17, Protocols for Determination of Limits of Detection and Limits of Quantitation described by Armbruster and Pry [37]. The limit of blank (LOB, L_{blank}) was calculated using (1), which was then used to calculate the LOD ($L_{detection}$) using (2).

$$L_{blank} = \mu_{blank} + 0.645(\delta_{blank}) \quad (1)$$

$$L_{detection} = L_{blank} + 1.645(\delta_{low\ conc.\ sample}) \quad (2)$$

Where μ_{blank} and δ_{blank} are the mean and standard deviations of the MPIs of the PBS control ROIs, and $\delta_{low\ conc.\ sample}$ is the standard deviation of the MPI of a low concentration dye ROI.

Linear regression lines of best fit were made for the MPIs as a function of concentration using data from 5 concentrations starting from one concentration below the LOB moving to higher concentrations (approx. 0 to approx. 25 μM). The MDC was estimated using the intersection of the linear regression line of best fit equation and the LOD. The following Eq. (3) was then rearranged to solve for the MDC:

$$LOD = m * MDC + b \quad (3)$$

where m and b are the slope and y-intercept respectively of the line of best fit.

The standard deviation was calculated from the line of best fit.

2.4.2. Linear range calculation

The linear range was determined through the statistical methods described in EP6-A [38]. The MPIs of QBB, dependent on the dye concentration, was fit with a model of a cubic function for the entire range of dye concentrations. If the coefficients of the cubic and/or quadratic terms were significantly different from zero ($P < 0.05$), then the plot of the MPI as a function of concentration was observed to remove data points from either the high concentration end or the low concentration end. The data was continuously fitted to the cubic function until the cubic and quadratic coefficients became non-significant. Subsequently, a quadratic function was fitted to the data and if the coefficient of the quadratic term was significantly different from zero, then the same steps of removing data were taken as mentioned previously until the quadratic term was non-significant. Finally, the linear model was estimated and the y-intercept and slope were derived. All analysis was completed using Microsoft Excel (Version 16, Point Roberts, WA) with the Data Analysis add-on.

2.4.3. Photoacoustic photostability analysis

To assess PA photostability, we imaged 25 μM of QBB at 750 nm (it's maximum NIR absorption wavelength) every 0.5 mm along the z-axis of the capillary tubes. A sample of 10 image slices per scan was selected for data analysis. The average and standard deviation MPI of the 10 slices for each of the three imaging samples were taken for each time point over 1 -h of laser exposure. The average MPI was then normalized to the maximum MPI and plotted as a function of time. A graph comparing the QBB PA photostability to that of other NIR dyes is shown in the Supplementary Material section 4 (SM Fig. 6). The 25 μM concentration was chosen since it is sufficiently higher than the MDC for all dyes tested. This is to avoid the PA laser photobleaching the dye samples so much so as to reduce the PA signal to zero. 25 μM is also a low enough concentration for all the tested dyes that the entire cross-section of the sample is illuminated.

2.5. BODIPY, dye for VIS fluorescence imaging

The results of the characterization experiments of the free NIR dyes (Supplementary Material 4), showed that neither of the tested fluorescent dyes had as steep a slope within their linear range nor could they withstand the repetitive PAI with minimal change in signal that QC-1 could. Therefore, we combined QC-1 with a fluorescent dye that absorbs and fluoresces outside the PAI range to prevent any PA or fluorescence photobleaching while maintaining the ability to detect the tracer with fluorescence imaging modalities. 4,4-Difluoro-4-bora-3a,4a-diaza-s-indacene dyes (known as boron dipyrromethenes, or BODIPYs) are robust in biological conditions, have high molar absorption coefficients and fluorescence quantum yields, narrow emission bandwidths with high peak intensities, good solubility, resistance towards self-aggregation in solution, and excitation/emission wavelengths in the visible (VIS) spectral region (500 nm), all of which contribute to the appeal of these interesting compounds [34]. These characteristics make them suitable for various fluorescence imaging applications [39,40]. BODIPY FL maleimide is a thiol-reactive dye that produces electronically neutral dye conjugates and was previously used for the quantification of labeled proteins [41,42]. The absorption max is at 500 nm which is below the wavelength range of the laser source of our PAI device. This avoids fluorescence photobleaching due to laser exposure during PAI. We conjugated BODIPY FL maleimide (ThermoFisher Scientific, ON, Canada) with QC-1/BSA as indicated by the supplier.

2.6. In vivo animal photoacoustic imaging with hybrid contrast agent

CD-1 albino mice (n = 3, male Charles River Laboratories, Canada) were injected with the 3 μL of 1 mM QBB tracer (calculated based on the concentration of QC-1) into the right subconjunctiva. The head and neck regions were imaged with the same PAI device prior to injection, and 10 min, 1 h and 2 h after injection. Images were reconstructed with the Backprojection algorithm and spectrally unmixed with the Adaptive Matched Filter algorithm in ViewMSOT.

2.7. Postmortem animal fluorescence imaging with hybrid contrast agent

After PAI, mice were sacrificed under general anesthesia, and the skin and fat of the head and neck region were removed to image *in situ* neck lymph nodes with a confocal scanning laser ophthalmoscopy (Spectralis, Heidelberg Engineering, Germany) for fluorescence detection of the QBB tracer.

After postmortem *in situ* imaging, the right and left neck lymph nodes were removed and processed for cryostat sectioning as previously described [7]. 20 μm thick cryosections were stained with DAPI (1:10000, ThermoFisher Scientific, Canada). Sections were then imaged with a confocal microscope (LSM700, Zeiss, Canada). Confocal images were taken using a 10x objective. Acquisition settings (laser intensity, pinhole size, gain) for the 405 channel (DAPI) and 488 channel (BODIPY) were consistent for all sections. Z-stacks of 15 μm thickness were collected with 1 μm step size. Images were processed using ImageJ software (NIH, Bethesda, MD) to create maximum intensity projections and color composites.

3. Results

3.1. Hybrid tracer preparation

The NIR nonfluorescent QC-1 and VIS fluorescent BODIPY derivative were conjugated to the BSA protein *via* the reactions shown in Fig. 1 A and B, respectively. The absorbance spectrum of the hybrid QBB tracer (Fig. 1 C) shows the absorbance peak for BODIPY and QC-1 at 500 nm and 750 nm, respectively, can confirm that both dyes were bound to albumin. The dye to protein ratios of QC-1 to BSA to BODIPY were 2.8:1:2, respectively, and the equations used to estimate these ratios can be found in Supplementary Material section 3.

3.2. In vitro Characterization

Photoacoustic and absorbance spectra of QBB are shown in Fig. 1 C. The MDC of QBB was calculated as 2.5 ± 0.19 μM (Fig. 2 A). The linear

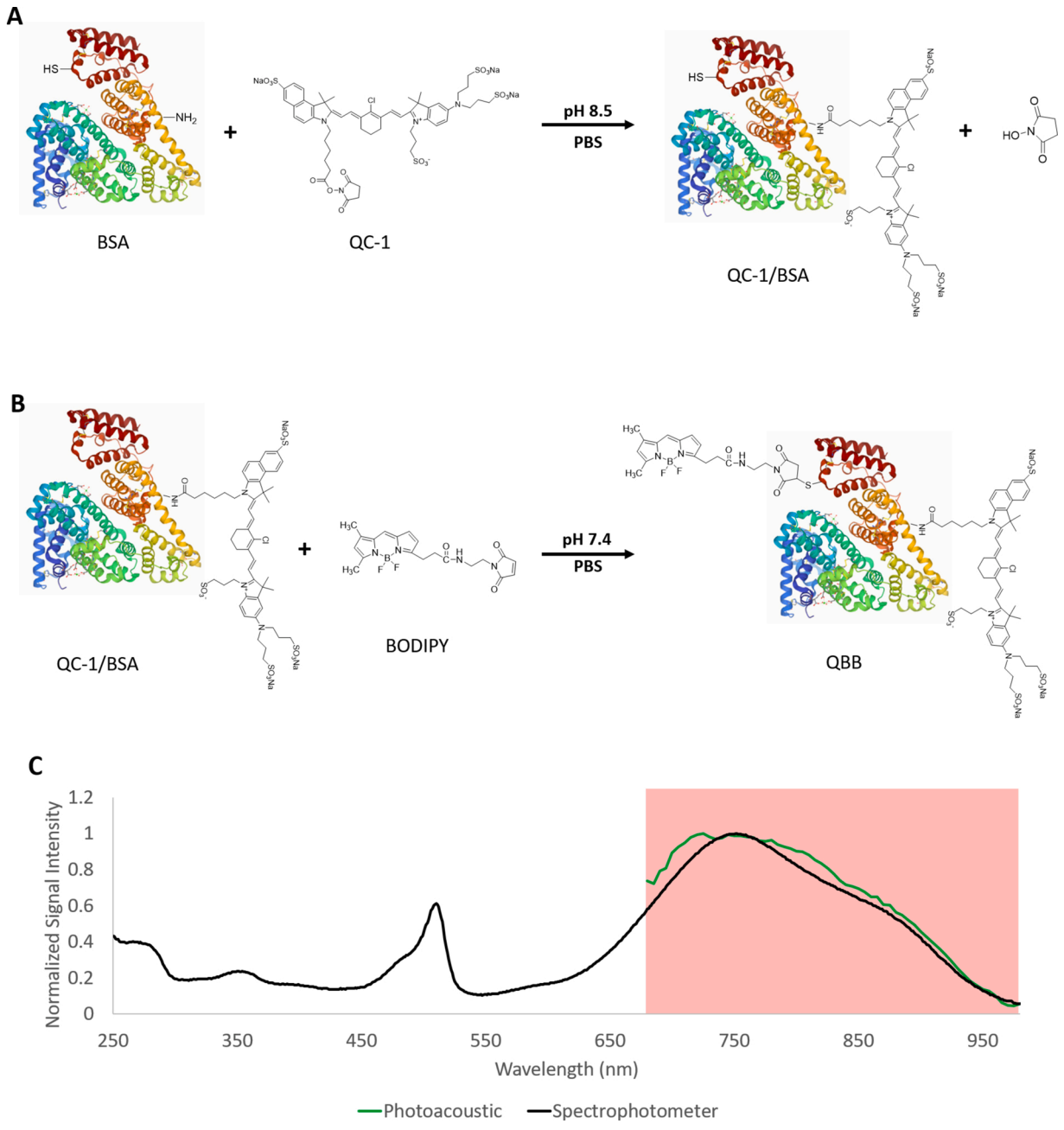

Fig. 1. A representation of the BSA labeling process to form the hybrid QBB tracer. A) The unbound bovine serum albumin (BSA) binding to IRDye QC-1 with an amine-ester bond. B) The QC-1-labelled BSA binding to BODIPY maleimide with a maleimide-thiol bond. Protein and dyes are not drawn to scale, the location of binding sites on BSA are not positioned accurately. BSA structural image was taken from the Protein Data Bank [43]. C) Normalized photoacoustic (green) and spectrophotometer absorbance (black) spectra of the QBB tracer. The region highlighted in red indicates the imaging wavelength range (680 nm to 980 nm) of the PAI system.

range was found between 2.4 and 54.4 μM with a slope of 3.39 E −5 as shown in Fig. 2 B. Lastly, after one hour of repetitive photoacoustic imaging, the QBB photoacoustic signal showed a decrease of approximately 10 % (Fig. 2 C).

Compared to the free NIR dyes we tested (Supplementary Material section 4) the QBB tracer had very similar characteristics to the free QC-1 dye. Both had similar slopes for their linear ranges and both had superior PA photostability compared to IRDye 800cw and CF770.

3.3. *In vivo and postmortem animal imaging*

The QBB tracer was immediately detected in the injected right eye for each of three mice with PAI as shown in Fig. 3. The tracer was also detected in the right neck lymph node of all three mice as early as 10 min after NIR tracer injection. The increase in PA signal, or MPI in the right neck lymph node over time compared to that in the left neck lymph node was seen in all three mice shown in Fig. 4. Postmortem *in situ* fluorescence imaging confirmed that the QBB tracer was located in the right neck lymph node with a confocal scanning laser ophthalmoscopy (Fig. 5) as well as in histology sections of the right neck lymph node using a confocal microscope (Fig. 6A). Minimal fluorescence signal was detected in the left neck node (Fig. 6B)

4. Discussion

In the present study, we designed and characterized a hybrid tracer

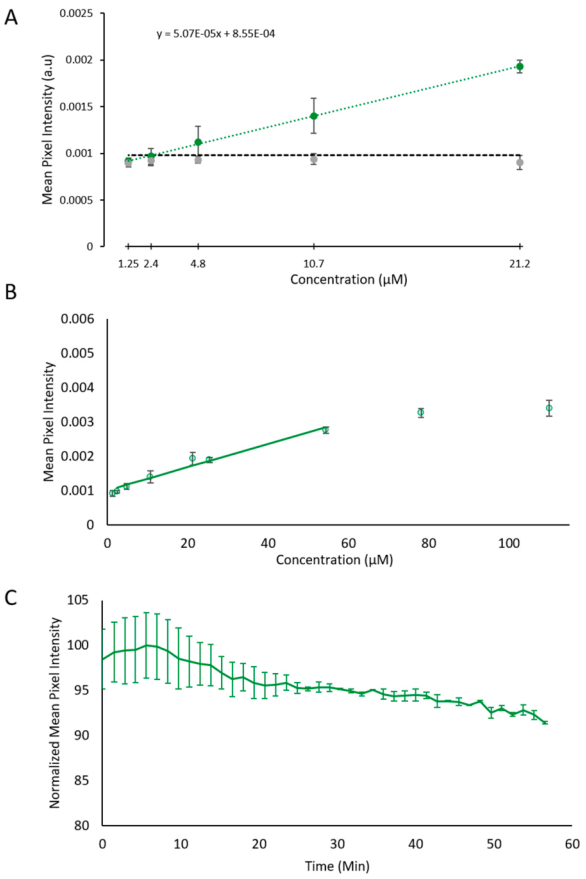

Fig. 2. A) Minimum detectable concentration (MDC) visualization graph of QBB. The dashed green line is the linear line of best fit of the lowest 5 concentrations. The dashed black line indicates the limit of detection. The intersection of the line of best fit and the limit of detection is the calculated MDC. B) The linear range plot of QBB is represented by the solid green line. QBB mean pixel intensity (MPI) data points with standard deviations are plotted for reference. C) The photoacoustic photobleaching of QBB where the MPI of QBB is plotted over time.

for NIR quantitative photoacoustic imaging and VIS fluorescence imaging. We also demonstrated in experiments performed in mice that the tracer can be used for *in vivo* quantitative PAI of the lymphatic drainage from the eye to neck lymph node over time and for the anatomic validation of the *in vivo* PAI findings using VIS fluorescence imaging.

The characteristics of the hybrid QBB tracer demonstrates the potential for use as an *in vivo* contrast agent for quantitative lymphatic PAI. The most notable PA characteristic of the QBB tracer being the relatively steep change in PA signal with concentration when compared to several other NIR dyes (IRDye 800CW, and CF770) characterized in this study (Supplementary Material section 4). This increases the sensitivity of PAI to changes in tracer concentration. Additionally, QBB demonstrated a relatively strong photostability compared to IRDye 800CW and CF770 allowing for more accurate measurements when a tracer will be exposed to sequential *in* vivo PAI for relevant studies.

Experiments after hybrid tracer injection in mice demonstrated that QBB is detected *in* vivo in the established lymphatic pathway and these *in* vivo PAI findings were validated by postmortem localization of the tracer in the draining lymph node using *ex vivo* fluorescence imaging. Slight variations in the PA MPI were observed across the three mice which could be attributed to inter-individual variability and quantifying

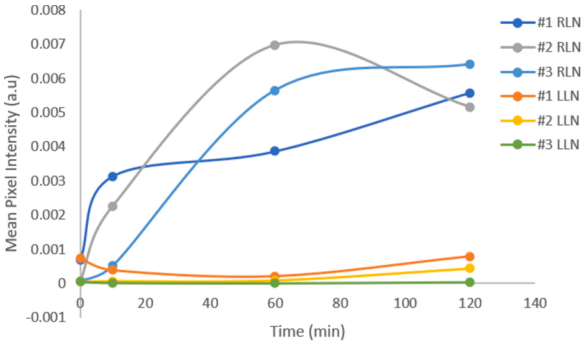

Fig. 4. Increase in QBB mean pixel intensity in the right neck lymph nodes (RLN) over time after tracer injection in the right eye compared to the left neck lymph nodes (LLN) in all three mice as indicated in the legend. The zero-time point corresponds to the imaging session just before the tracer injection.

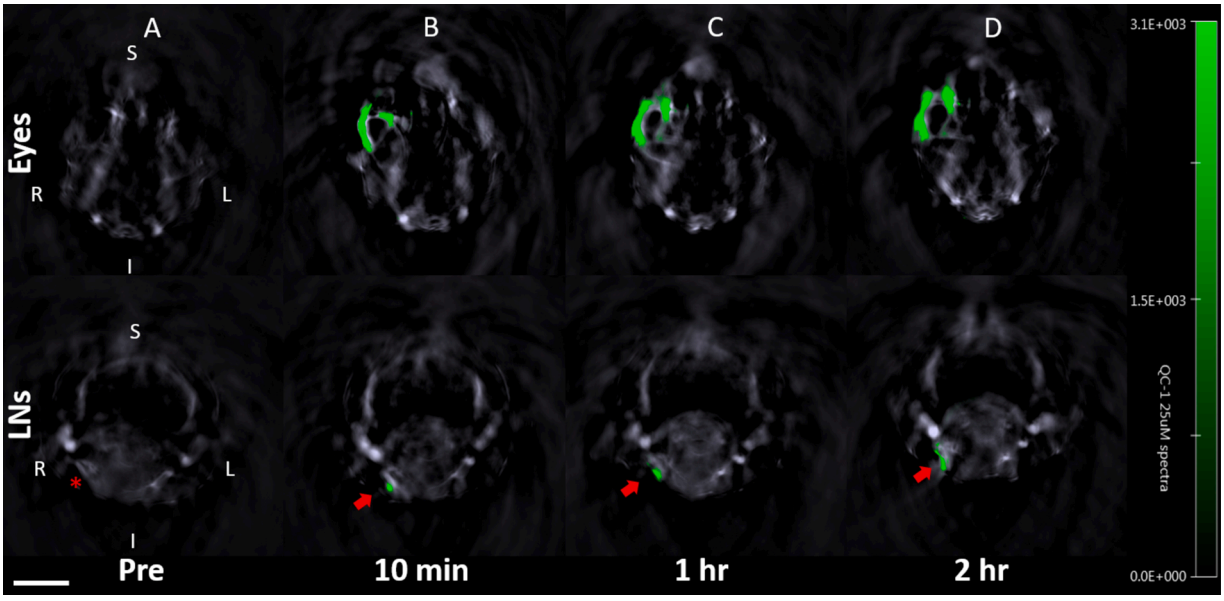

Fig. 3. Photoacoustic cross-sectional images of the head at the level of the eyes (top row) and neck region (bottom row) of an albino CD-1 mouse (ID#1) after injection of 3 μL of 1 mM QBB. The green pixels indicate the presence of the QBB tracer. R = right; L = left; S = superior; I = inferior. Scale bar =5 mm. The red asterisk indicates the location of the right neck lymph node. Red arrows indicate the right neck lymph node with the QBB signal in green.

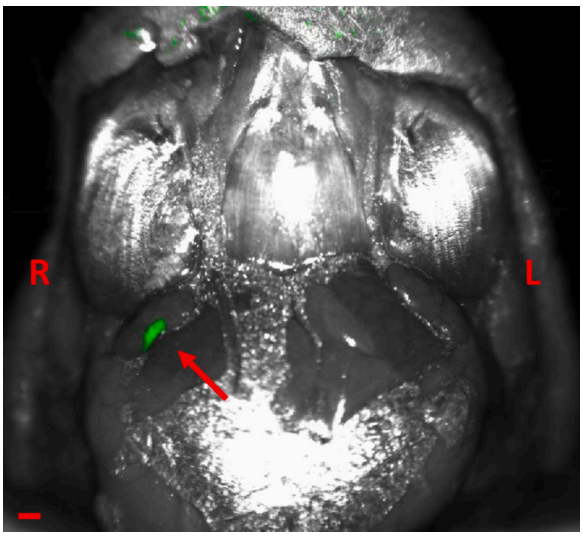

Fig. 5. Postmortem *in situ* fluorescence image of the ventral view of the neck after removal of skin and fat. Green pixels show fluorescence (486 nm wavelength) signal of the hybrid tracer in the right neck lymph node (arrow). No fluorescence signal is detected in the left neck lymph node. R and L indicate the right and left sides. The scale bar indicates 200 μm.

the fluorescence signal from the QBB tracer could potentially show similar variability. However, the focus of this study was to design a tracer for quantifying PA signal *in vivo* and using the fluorescence as a verification for the location of the tracer postmortem. Additionally, the photostability of the QBB under fluorescence imaging conditions was not tested since the fluorescence imaging was used postmortem for scan times that lasted on the order of seconds. However, if QBB were to be used with a hybrid PA and fluorescence imaging device for *in vivo* quantitative fluorescence imaging as well as PAI, the fluorescence photostability would need to be characterized. Future studies using this tracer can be implemented to compare quantitatively the PA signal with fluorescence signal *in vivo*. Furthermore, using higher sensitivity fluorescence detection systems may enable quantitative analysis of the fluorescence signal.

The use of this hybrid tracer QBB has the potential to quantify changes in the lymphatic drainage from the eye, brain, and systemic organs. QBB could be used as a PAI contrast agent for other applications including, but not limited to, lymphatic imaging for cancer research. Other carriers such as other proteins and biologics can be dual labeled with QC-1 and BODIPY and this approach can be adapted to other biomedical applications.

We also described a systematic, non-biased method of characterizing contrast agents for use in quantitative PAI based on well-established statistical methods [37,38]. These methods determined the quantitative characteristics of contrast agents including their MDC, or sensitivity, and linear range of concentrations. Furthermore, the PA photostability has been performed before in various other studies [44–46] was also used to characterize our hybrid tracer and several free NIR dyes. PA photostability, defined by a percent change in the photoacoustic signal generation as a function of laser exposure, or PAI time, is a characteristic that may interfere with sequential quantitative studies.

The characterization methods were applied to select the optimal NIR dye from an, albeit limited, selection of commercial dyes for use in *in vivo* PAI and postmortem fluorescence validation in the same animal. Results found in the Supplementary Material Section 4 demonstrated that the NIR QC-1 quencher is more photostable compared to the tested fluorescent NIR dyes and suitable for sequential imaging sessions after tracer injection of the same animal for quantitative PAI over time.

When it comes to the specific detection and quantification of PA contrast agents, spectral analysis techniques are relevant [47–50]. Spectral unmixing is particularly necessary in *in vivo* settings, with complex 3D-anatomy and increasing tissue depth, tissue optics, biological variation, and endogenous chromophores (*e.g.* hemoglobin) which produce complex background signal [48,49,51,52]. For validation of the location and the amount of contrast agent measured in target during PAI, postmortem localization, and quantitative measurement of the contrast agent is required for comparing various contrast agents. VIS fluorescence imaging modalities such as fluorescence imaging and microscopy are readily available for *in situ* imaging and histological imaging, respectively.

QC-1, selected for quantitative PAI following a standardized comparison of multiple NIR dyes, was conjugated to an albumin carrier bound with a VIS fluorescent dye, BODIPY. This hybrid contrast agent enables quantitative PAI of lymphatic drainage and postmortem

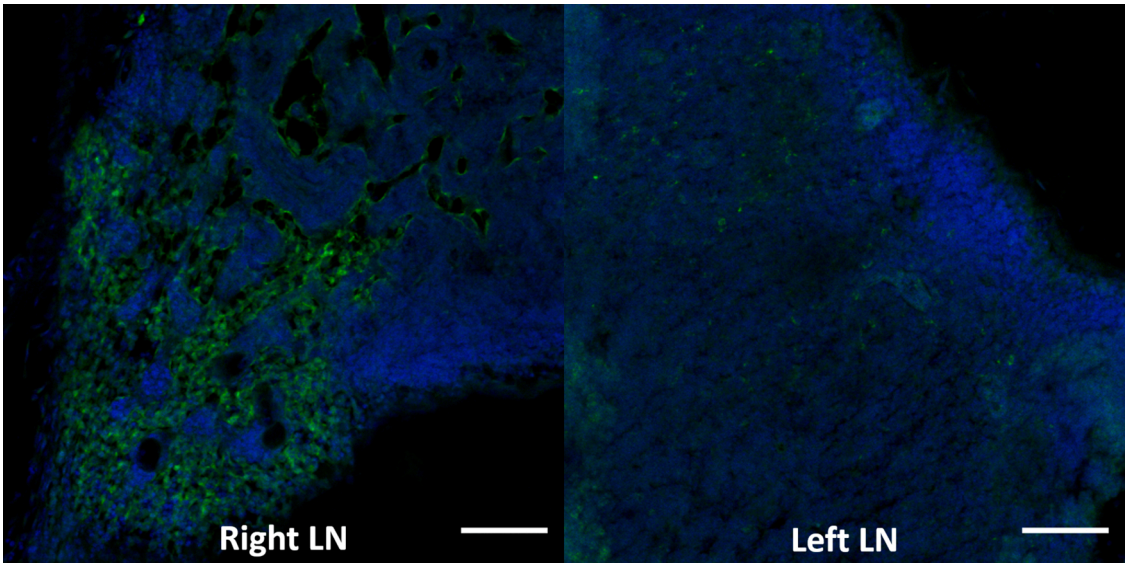

Fig. 6. Right (ipsilateral to the injected eye) and left neck lymph node sections counterstained with a nuclear stain DAPI (blue) imaged with a confocal microscope. The green signal shows the location of the hybrid tracer QBB in the right neck lymph node (LN). Minimal fluorescence signal is noted in the left neck lymph node. Green =488 nm for the QBB fluorescence signal, Blue =405 nm for the DAPI signal. The scale bars indicate 200 μm.
iversity of Waterloo (2000), and PhD at the Universit

validation using fluorescence imaging with readily available fluorescence optical devices.

Previously, Madea et al. dually labeled a VIS quencher dye and VIS fluorescent dye to the same antibody for the use of photoacoustic and fluorescence imaging [53]. The selected fluorescent dye (NHS-fluorescein) had a similar emission wavelength to our selected BODIPY dye. However, the selected VIS quencher dye, Black hole quencher 3 (BHQ-3) had a peak absorption wavelength of 612 nm in solution which was outside the NIR PAI range and therefore reduced its effectiveness as a PA contrast agent. In our study, the selected quencher dye, QC-1, has a peak absorption wavelength well within the NIR PAI range that allows improved signal to noise ratio and greater penetration depth. Furthermore, the fluorescent dye BODIPY used in our study has a larger molar extinction coefficient and higher quantum yield than fluorescein which makes it more sensitive to postmortem detection by fluorescence imaging [54]. The addition of the BODIPY dye did not interfere significantly with the PA spectrum of QC-1 and maintained the VIS fluorescence after tissue fixation. BODIPY was detected with *in situ* fluorescence imaging and microscopy in the lymph nodes sections, respectively.

Another more recent study created an activatable polymeric reporter for PA and fluorescence imaging to target malignant breast cancer [55]. However, this type of contrast agent was designed to target cancer and does not enable the tracing ability that non-activatable probes such as QBB allow. The same group also used semiconducting polymer nanoparticles that allow for dual-modality PA and fluorescence imaging [56, 57]. There are several benefits to using metallic or semiconducting nanostructures as PA and fluorescent contrast agents including but not limited to their photostability and their flexibility in terms of chemical and physical properties [17]. However, by using relatively small dyes like QC-1 and BODIPY, we are able to maintain the properties of the native albumin protein to minimize the risk of potential toxicity concerns or an immune response. Furthermore, as the physio-chemical characteristics of albumin are well known [58], the QBB tracer obtained by covalently binding two dyes with low molecular weight and a low dye/protein ration to albumin may not require in deep characterization using transmission electron microscopy, zeta potential, and dynamic light scattering that would be needed for novel newly synthesized nanoparticles [59].

When the hybrid tracer was tested in the *in vivo* mouse model of lymphatic imaging settings, QBB injected in the right eye was detected in the right neck lymph node with PAI and the tracer signal in the right neck node increased over time. However, due to the small sample size, no conclusions can be made on the rate of PA tracer accumulation in the lymph nodes as done previously [7]. *Ex vivo* and *in situ*, VIS fluorescence imaging using a confocal scanning laser imager validated the i*n vivo* QBB signal localized in the draining right neck lymph node. Confocal microscopy imaging of lymph nodes sections counterstained with a fluorescent nuclear marker demonstrated that QBB was located in the draining right neck lymph node and minimally in the left lymph node. These two fluorescence imaging modalities of the postmortem tissue material validated that the signal detected by i*n vivo* PA tracer signal located in the right neck region was located in the right neck lymph node using postmortem fluorescence imaging and microscopy.

Future efforts can be aimed towards using hybrid tracers such as QBB in *in vivo* experiments similar to those used lymphatic drainage of the brain and tumors [7,20] with the qualitative anatomical histological validation in the same mice. Additionally, further characterization of QBB for fluorescence photostability over light exposure with sensitive quantitative fluorescence measurement systems could provide insight on the effectiveness of the hybrid tracer for repetitive, quantitative *in vivo* fluorescence imaging. Furthermore, since there is a frequent output of new NIR dyes, various other hybrid tracers could be made and tested using the *in vitro* and statistical methods used in this study.

5. Conclusion

Dual labeling albumin with QC-1, a dark quencher, and BODIPY, a VIS fluorescent dye (QBB) has the potential to provide non-invasive quantitative PAI of lymphatic clearance over time and anatomical and histological validation using postmortem *in situ* fluorescence imaging and microscopy. Here, the developed systematic approach for rational screening a variety of NIR dyes based on quantitative criteria allowed us to compare and identify the best performing PA agents.

Specifically, we observed that there are stark variations in NIR dye performance, highlighting the importance of developing new and better contrast agents for PAI technology. Albumin bioconjugation provides a stable and facile solution for the delivery of hydrophobic dyes to the lymphatic system. We have demonstrated in a mouse model that QBB is a highly potent PAI agent for quantitative lymphatic imaging. Not only is our albumin-based platform suitable for NIR PAI, but it also allows postmortem validation. This new contrast agent and the standardized methods to compare various photoacoustic agents, and detection and quantification methods have the potential to translate to other biomedical applications of PAI, encompassing other eye and brain diseases and cancer. This category of PA-fluorescent hybrid organic contrast agent alongside the other hybrid contrast agents cited in this paper could be beneficial in the development and improvement of existing PA-fluorescent imaging systems for potential clinical use.

Declaration of Competing Interest

The research presented in this paper was conducted as a part of Kirsten Cardinell's Biomedical Physics MSc at Ryerson University. Currently, she is employed at iThera Medical GmbH.

Acknowledgments

This work was supported by grants from the Canadian Institutes of Health Research (MOP119432; YHY, NG; Ottawa, ON, Canada), the Canada Foundation for Innovation Leaders Opportunity Fund (31326; YHY; Ottawa, ON, Canada), the Glaucoma Research Society of Canada (NG, YHY; Toronto, ON, Canada), Alayne and Ron Metrick Research Fund, Keenan Family Research Foundation, (NG; Toronto, ON, Canada), the Henry Farrugia Research Fund (YHY; Toronto, ON, Canada), and Natural Sciences and Engineering Research Council of Canada - Canada Graduate Scholarships-Master's Program (KC; Ottawa, ON, Canada).

Appendix A. Supplementary data

Supplementary material related to this article can be found, in the online version, at doi:https://doi.org/10.1016/j.pacs.2021.100239.

References

[1] V. Mumprecht, M. Detmar, Lymphangiogenesis and cancer metastasis, J. Cell. Mol. Med. 13 (2009) 1405–1416.
[2] J. Wilting, J. Becker, K. Buttler, H. Weich, Lymphatics and inflammation, Curr. Med. Chem. 16 (2009) 4581–4592.
[3] P. Moriguchi, et al., Lymphatic system changes in diabetes mellitus: role of insulin and hyperglycemia, Diabetes Metab. Res. Rev. 21 (2005) 150–157.
[4] N.L. Harvey, et al., Lymphatic vascular defects promoted by Prox1 haploinsufficiency cause adult-onset obesity, Nat. Genet. 37 (2005) 1072–1081.
[5] Y.H. Yücel, et al., Identification of lymphatics in the ciliary body of the human eye: a novel 'uveolymphatic' outflow pathway, Exp. Eye Res. 89 (2009) 810–819.
[6] A.L.C. Tam, N. Gupta, Z. Zhang, Y.H. Yücel, Latanoprost stimulates ocular lymphatic drainage: an in vivo nanotracer study, Transl. Vis. Sci. Technol. 2 (2013) 3.
[7] Y.H. Yücel, et al., Active lymphatic drainage from the eye measured by noninvasive photoacoustic imaging of near-infrared nanoparticles, Investig. Ophthalmol. Vis. Sci. 59 (2018) 2699–2707.
[8] G.P. Luke, et al., Silica-coated gold nanoplates as stable photoacoustic contrast agents for sentinel lymph node imaging, Nanotechnology (2013), https://doi.org/10.1088/0957-4484/24/45/455101.
[9] G.P. Luke, J.N. Myers, S.Y. Emelianov, K.V. Sokolov, Sentinel lymph node biopsy revisited: ultrasound-guided photoacoustic detection of micrometastases using

molecularly targeted plasmonic nanosensors, Cancer Res. (2014), https://doi.org/10.1158/0008-5472.CAN-14-0796.
[10] G.P. Luke, S.Y. Emelianov, Label-free detection of lymph node metastases with US-guided functional photoacoustic imaging, Radiology (2015), https://doi.org/10.1148/radiol.2015141909.
[11] M. Pramanik, et al., In vivo photoacoustic (PA) mapping of sentinel lymph nodes (SLNs) using carbon nanotubes (CNTs) as a contrast agent, Proc. SPIE 7177 (2009), 71771N.
[12] C. Lee, et al., Dual-color photoacoustic lymph node imaging using nanoformulated naphthalocyanines, Biomaterials 73 (2015) 142–148.
[13] D. Pan, et al., Near infrared photoacoustic detection of sentinel lymph nodes with gold nanobeacons, Biomaterials 31 (2010) 4088–4093.
[14] Z. Liu, et al., Dual-modality noninvasive mapping of sentinel lymph node by photoacoustic and near-infrared fluorescent imaging using dye-loaded mesoporous silica nanoparticles, Mol. Pharm. 12 (2015) 3119–3128.
[15] D. Pan, et al., Photoacoustic sentinel lymph node imaging with self-assembled copper neodecanoate nanoparticles, ACS Nano 6 (2012) 1260–1267.
[16] G.P. Luke, D. Yeager, S.Y. Emelianov, Biomedical applications of photoacoustic imaging with exogenous contrast agents, Ann. Biomed. Eng. (2012), https://doi.org/10.1007/s10439-011-0449-4.
[17] J. Weber, P.C. Beard, S.E. Bohndiek, Contrast agents for molecular photoacoustic imaging, Nat. Methods 13 (2016) 639–650.
[18] Z. Liu, X. Chen, Simple bioconjugate chemistry serves great clinical advances: albumin as a versatile platform for diagnosis and precision therapy, Chem. Soc. Rev. (2016), https://doi.org/10.1039/c5cs00158g.
[19] C.A. Davies-Venn, et al., Albumin-binding domain conjugate for near-infrared fluorescence lymphatic imaging, Mol. Imaging Biol. 14 (2012) 301–314.
[20] Y.H. Yücel, F. Cheng, K. Cardinell, X. Zhou, H. Irving, Age-related decline of lymphatic drainage from the eye : a noninvasive in vivo photoacoustic tomography study Age-related decline of lymphatic drainage from the eye : a noninvasive in vivo photoacoustic tomography study, Exp. Eye Res. 194 (2020), 108029.
[21] L.J. Rich, M. Seshadri, Photoacoustic imaging of vascular hemodynamics: validation with blood oxygenation level–dependent MR imaging, Radiology 275 (2014) 110–118.
[22] J. Kang, et al., Photoacoustic imaging of breast microcalcifications: a validation study with 3-dimensional ex vivo data and spectrophotometric measurement, J. Biophotonics 8 (2015) 71–80.
[23] J.R. Cook, W. Frey, S. Emelianov, Quantitative photoacoustic imaging of nanoparticles in cells and tissues, ACS Nano 7 (2013) 1272–1280.
[24] L. Nie, et al., Palladium nanosheets as highly stable and effective contrast agents for in vivo photoacoustic molecular imaging, Nanoscale 6 (2014) 1271–1276.
[25] S.A. Ermilov, et al., Laser optoacoustic imaging system for detection of breast cancer, J. Biomed. Opt. 14 (2009), 024007.
[26] S. Manohar, et al., Initial results of in vivo non-invasive cancer imaging in the human breast using near-infrared photoacoustics, Opt. Express 15 (2007) 12277.
[27] S. Mallidi, K. Watanabe, D. Timerman, D. Schoenfeld, T. Hasan, Prediction of tumor recurrence and therapy monitoring using ultrasound-guided photoacoustic imaging, Theranostics 5 (2015) 289–301.
[28] R. Alford, et al., Toxicity of organic fluorophores used in molecular imaging: literature review, Mol. Imaging (2009).
[29] Y.S. Chen, Y.C. Hung, I. Liau, G.S. Huang, Assessment of the in vivo toxicity of gold nanoparticles, Nanoscale Res. Lett. 4 (2009) 858–864.
[30] J.K. Fard, S. Jafari, M.A. Eghbal, A review of molecular mechanisms involved in toxicity of nanoparticles, Adv. Pharm. Bull. (2015), https://doi.org/10.15171/apb.2015.061.
[31] J. Laufer, A. Jathoul, M. Pule, P. Beard, In vitro characterization of genetically expressed absorbing proteins using photoacoustic spectroscopy, Biomed. Opt. Express 4 (2013) 2477.
[32] S. Roberts, et al., Acid specific dark quencher QC1 pHLIP for multi-spectral optoacoustic diagnoses of breast cancer, Sci. Rep. 9 (2019) 1–12.
[33] S. Roberts, et al., Sonophore-enhanced nanoemulsions for optoacoustic imaging of cancer, Chem. Sci. 9 (2018) 5646–5657.
[34] N.N. Boens, V. Leen, W. Dehaen, Fluorescent indicators based on BODIPY, Chem. Soc. Rev. 41 (2012) 1130–1172.
[35] W.S. Tummers, et al., Intraoperative pancreatic Cancer detection using tumor-specific multimodality molecular imaging, Ann. Surg. Oncol. 25 (2018) 1880–1888.
[36] C. Kim, K.H. Song, F. Gao, L.V. Wang, Sentinel lymph nodes and lymphatic vessels: noninvasive dual-modality in vivo mapping by using indocyanine green in rats—volumetric spectroscopic photoacoustic imaging and planar fluorescence imaging, Radiology 255 (2010) 442–450.
[37] D. Armbruster, T. Pry, Limit of blank, limit of detection and limit of quantitation, Clin. Biochem. Rev. 29 (2008) 49–52.
[38] D. Tholen, et al., EP06-a evaluation of the linearity of quantitative measurement procedures: a statistical approach; approved guideline, in: CLSI Documents EP06-A, 23, 2003.
[39] T. Kowada, H. Maeda, K. Kikuchi, BODIPY-based probes for the fluorescence imaging of biomolecules in living cells, Chem. Soc. Rev. (2015), https://doi.org/10.1039/c5cs00030k.
[40] D. Su, C.L. Teoh, S. Sahu, R.K. Das, Y.T. Chang, Live cells imaging using a turn-on FRET-based BODIPY probe for biothiols, Biomaterials (2014), https://doi.org/10.1016/j.biomaterials.2014.04.035.
[41] B.G. Hill, C. Reily, J.Y. Oh, M.S. Johnson, A. Landar, Methods for the determination and quantification of the reactive thiol proteome, Free Radic. Biol. Med. (2009), https://doi.org/10.1016/j.freeradbiomed.2009.06.012.
[42] K. Tyagarajan, E. Pretzer, J.E. Wiktorowicz, Thiol-reactive dyes for fluorescence labeling of proteomic samples, Electrophoresis 24 (2003) 2348–2358.
[43] K.A. Majorek, et al., Crystal Structure of Bovine Serum Albumin, 2012, https://doi.org/10.2210/pdb3V03/pdb.
[44] W. Mahmood Mat Yunus, K.S. Chan, W.M. Zin Wan Yunus, Study on photobleaching of methylene blue doped in PMMA, PVA and gelatin using photoacoustic technique, J. Nonlinear Opt. Phys. Mater. 12 (2003) 91–100.
[45] N.A. George, B. Aneeshkumar, P. Radhakrishnan, C.P.G. Vallabhan, Photoacoustic study on photobleaching of Rhodamine 6G doped in poly(methyl methacrylate), J. Phys. D Appl. Phys. 32 (1999) 1745–1749.
[46] R. Carpentier, R.M. Leblanc, M. Mimeault, Photoinhibition and chlorophyll photobleaching in immobilized thylakoid membranes, Enzyme Microb. Technol. 9 (1987) 489–493.
[47] S. Tzoumas, et al., Eigenspectra optoacoustic tomography achieves quantitative blood oxygenation imaging deep in tissues, Nat. Commun. (2016), https://doi.org/10.1038/ncomms12121.
[48] S. Morscher, et al., Spectral unmixing using component analysis in multispectral optoacoustic tomography, Optics InfoBase Conference Papers (2011), https://doi.org/10.1117/12.889415.
[49] J. Glatz, N.C. Deliolanis, A. Buehler, D. Razansky, V. Ntziachristos, Blind source unmixing in multi-spectral optoacoustic tomography, Opt. Express (2011), https://doi.org/10.1364/oe.19.003175.
[50] S. Tzoumas, A. Nunes, N.C. Deliolanis, V. Ntziachristos, Effects of multispectral excitation on the sensitivity of molecular optoacoustic imaging, J. Biophotonics (2015), https://doi.org/10.1002/jbio.201400056.
[51] S. Tzoumas, V. Ntziachristos, Spectral unmixing techniques for optoacoustic imaging of tissue pathophysiology, Philos. Trans. A Math. Phys. Eng. Sci. 375 (2017) 20170262.
[52] G.P. Luke, S.Y. Nam, S.Y. Emelianov, Optical wavelength selection for improved spectroscopic photoacoustic imaging, Photoacoustics 1 (2013) 36–42.
[53] A. Maeda, J. Bu, J. Chen, G. Zheng, R.S. DaCosta, Dual in vivo photoacoustic and fluorescence imaging of HER2 expression in breast tumors for diagnosis, margin assessment, and surgical guidance, Mol. Imaging 14 (2018), 7290.2014.00043.
[54] O. Green, et al., BODIPY Dye Series — Section 1. 4. 1–12, 2019.
[55] Q. Li, et al., An activatable polymeric reporter for near-infrared fluorescent and photoacoustic imaging of invasive cancer, Angew. Chemie - Int. Ed. 59 (2020) 7018–7023.
[56] D. Cui, et al., Thermoresponsive semiconducting polymer nanoparticles for contrast-enhanced photoacoustic imaging, Adv. Funct. Mater. 29 (2019), 1903461.
[57] Y. Jiang, K. Pu, Multimodal biophotonics of semiconducting polymer nanoparticles, Acc. Chem. Res. 51 (2018) 1840–1849.
[58] U. Kragh-Hansen, Chapter 1 human serum albumin: a multifunctional protein, in: M. Otagiri, V.T.G. Chuang (Eds.), Albumin in Medicine: Pathological and Clinical Applications, Springer, Singapore, 2016, pp. 1–25, https://doi.org/10.1007/978-981-10-2116-9.
[59] Y. Iwao, Chapter 5 albumin nanoparticles, in: M. Otagiri, V.T.G. Chuang (Eds.), Albumin in Medicine: Pathological and Clinical Applications, Springer, Singapore, 2016, pp. 91–100, https://doi.org/10.1007/978-981-10-2116-9.

Kirsten Cardinell received a B.Sc in Medical Physics in 2017 and a M.Sc. degree in Biomedical Physics in 2019 from the Faculty of Science at Ryerson University, Toronto. She is currently a field service engineer for iThera Medical.

Dr. Gupta is a surgeon-scientist with the Keenan Research Centre for Biomedical Science at the University of Toronto where she directs a translational research team that has published numerous seminal scientific articles focused on visual system injury in glaucoma and new treatments. She has played an integral role in the discovery of brain changes in glaucoma and translating the findings to human disease. For her groundbreaking work, she received the World Glaucoma Association Award. Her team discovered the lymphatic circulation in the eye, awarded the New York Academy of Medicine Lewis Rudin Glaucoma Research Prize. Her research contributions have been recognized by election to the Glaucoma Research Society composed of international glaucoma scholars with 86 active members http://www.glaucomasociety.org/.'

J. Carl Kumaradas received his M.A.Sc.degree in Electrical Engineering from the University of Toronto in 1993 and his M. Sc. and Ph.D. degrees in Biomedical Physics from the University of Toronto in 1996 and 2002, respectively. He was a Postdoctoral Associate in Biophysics at Los Alamos National Laboratory from 2002 to 2004. Since 2004 he has been working as an Assistant and then Associate Professor in the Department of Physics at Ryerson University and is the Associate Dean of Graduate Programs. He worked on microwave based thermal therapy as an adjuvant for radiotherapy during his graduate studies and magnetic nanoparticle based thermal therapy during his Postdoctoral work. He currently focuses on acoustic and photoacoustics imaging and the use of gold nanoparticles in for thermal therapy and radiotherapy. His expertise is in the development and implementation of computational models for these applications.

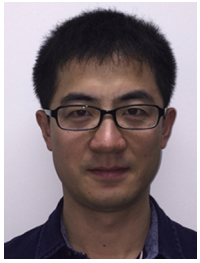

Xun Zhou received his M.Sc. degree in Neuroscience from University of Ottawa, Canada in 2011. He worked as a research technician at Ottawa Hospital Research Institute from 2011 to 2015. He is currently a research technician at the Keenan Research Centre for Biomedical Science of St. Michael's Hospital in Toronto, Canada. His research interests are neurodegenerative diseases and lymphatic drainage in the brain and eye.

Hyacinth Irving is a biostatistician at the Centre for Global Health Research, St. Michael's Hospital, Toronto, Canada. Her current work focuses on estimating tobacco attributable mortality in Ontario and Latin America.

Paola Luciani is Full Professor of Pharmaceutical Technology at the University of Bern, Switzerland. She obtained her M.Sc. and Ph.D. in Chemical Sciences at the University of Rome La Sapienza in 2002 and 2006, respectively, and subsequently worked as research fellow on colloidal sciences at the University of Florence. In 2009 she joined the Drug Delivery and Formulation Group headed by Prof. Leroux at ETH Zurich, Switzerland, as postdoctoral scientist and later as group leader. In 2015 she was appointed Associate Professor for Phospholipids in Drug Development at the University of Jena, Germany. Her current research focuses on the design and characterization of lipid-derived delivery systems and of biocompatible contrast agents for *in vivo* imaging.

Yeni Yucel MD, MSc, PhD, FRCPC(Neuropath) MD, MSc and PhD in Neuroscience from the University of Strasbourg, CNRS, France, 1985, 1986 and 1989, respectively. Postdoctoral fellowship at the University of British Columbia, and Hospital for Sick Children, Canada. Neuropathology Residency, FRCPC (Neuropath) at the University of Toronto, Canada. Research fellowship at the University of California, San Diego, USA. He is currently Professor and Director of Ophthalmic Pathology, Department of Ophthalmology and Vision Sciences, Department of Laboratory Medicine & Pathobiology, University of Toronto. He is also Founding Director, Human Eye Biobank for Research. He is a Member, Institute of Biomedical Engineering Science and Technology (iBEST) and an Adjunct Professor, Physics, Faculty of Science and Faculty of Engineering and Architectural Science, Ryerson University. Research interests include application of tissue optics for noninvasive imaging and for experimental and clinical pathology, fluid dynamics within and around the eye, lymphatics, and neurodegeneration.

Bryan D. Koivisto, Associat Professor. After finishing his BSc at the University of Waterloo (2000), and PhD at the University of Victoria (2006), Dr. Koivisto held an NSERC PDF position at the University of Edinburgh investigating the utility of molecular machines for light harvesting (2006-2008). Dr. Koivisto then joined the Institute for Sustainable Energy, Environment and Economy at the University of Calgary (2008-2011). There he continued to focus his research interests by investigating the conversion of light energy into solar fuels. In 2011, Dr. Koivisto joined the Department of Chemistry and Biology at Ryerson University (Toronto, Canada). As an associate member of Ryerson's Centre for Urban Energy, Dr. Koivisto's work investigates *the design and fabrication of dye-sensitized solar cells using bio-inspired light-harvesting dyes.*Since 2011, Bryan has established a vigorous research program to better appreciate the utility of organic dyes light-harvesting. After receiving promotion to Associate Professor in 2014, Dr. Koivisto has continued to embrace mentorship and innovation in scientific discovery, and has developed a number of programs designed to promote interdisciplinary evidence-based experiential learning. As such, he was the founding Director of the Science Discovery Zone (May 2016 – May 2019); a non-traditional incubation ecosystem hosted at Ryerson University.